

# The Implementation of Sapphire Microreflector for Monolithic Micro-LED Array

Chengshiu Liou<sup>1</sup>, Fuchi Shih, Yuanyuan Huang, Zihong Hu, Chingfu Tsou<sup>1</sup>,  
and Weileun Fang<sup>2</sup>, *Fellow, IEEE*

**Abstract**—This article proposed a novel design for the monolithic micro-LED array, directly integrated with a sapphire microreflector. Its resolution was 300 dpi. Theoretically, each micro-LED pixel owns an individual sapphire microreflector which can directly concentrate rays from an emitting source. Therefore, this study proposed that the optical crosstalk between neighboring micro-LED pixels could be suppressed and the contrast of the micro-LED array improved; as this would be especially beneficial for display. The simulation results showed that the increased thickness of the sapphire microreflector could further improve the optical performance of the micro-LED array. For the fabrication process, the key technology was an integrated process involving the inductively coupled plasma (ICP) etching technology for sapphire and micro-LED fabrication, which was used to fulfill the proposed and reference micro-LED arrays. The measurement results showed that the sapphire microreflector could effectively concentrate the emitting rays and increase the contrast of the micro-LED array. In addition, it also indicated that the inclination angle of the microreflector could further improve optical performance. Therefore, this approach was verified to be capable of improving the performance of the micro-LED display.

**Index Terms**—Inductively coupled plasma (ICP) etching technology, monolithic micro-LED array, sapphire microreflector.

## I. INTRODUCTION

IN THE past decades, there has been a rapid development in the technology of inorganic light emitting diodes (LEDs), with varieties of emitting wavelength, high brightness, and high efficiency, which was specially optimized by a growth method of GaN-based compounds and surface treatment on GaN-based structure or sapphire substrate [1]–[3]. LEDs were used to replace traditional light sources, such as the cathode

ray tube (CRT) and compact fluorescent lamp (CFL), and have been applied as the main emitting source in most optoelectronic applications and productions. In recent years, the prospects of micro-LED display technology as the display technique for the next generation have been high, especially as it has all the advantages of OLED displays and an even longer lifetime. Based on mature microfabrication, there are two types of micro-LED devices suitable for different approaches to the pixel assembly process. For one type, the individual microdevice divides from epi-wafer, and then it is precisely transferred on the circuit board to complete the display [4]. However, in recent times, there have been production cost and accuracy limitations with regard to manufacturing equipment and measurement, respectively. The second type is the monochromatic micro-LED array, which consists of GaN-based materials on sapphire substrate and shares a common-N interconnection, assembled on a circuit board using monolithic array integration [5]. This type can be relatively simple and easy to implement in mass production. Besides, the pixel density on the array can be more than 2000 dpi and it meets high-resolution requirements, such as is required for smartphones, smartwatches, tablets, augmented reality/mixed reality (AR/MR), laptops, televisions, head-up displays, and projection microdisplays.

However, there are still some issues with micro-LED arrays that researchers and developers have striven to overcome. For example, to make the pixels have uniform emission intensity and nearly consistent forward voltage, the path resistance was reduced by replacing the interconnection of the common cathode to a metal line with high conductivity [6]. Besides, full-color display is one of the main issues encountered with LEDs, hence, some persons vertically stack different monochromatic micro-LED arrays, and then independently control the pixels for color mixing [7]; others utilize quantum-dots (QDs) excited optically by blue or ultraviolet (UV) light source to realize color conversion [8]. In addition, the Lambertian illuminance distribution of LED characteristics is something that needs to be considered. When the neighboring pixels on the array are simultaneously driven, optical crosstalk takes place, which decreases the contrast between adjacent pixels. Moreover, the efficiency of a single pixel also decreases due to the fact that some of the emitting rays are distributed to undesired areas. Therefore, the grid black mold is assembled on the micro-LED array to shadow the emitted light with a wide angle [9].

Manuscript received October 13, 2020; revised December 21, 2020; accepted December 24, 2020. Date of publication January 6, 2021; date of current version February 17, 2021. This work was supported by the Ministry of Science and Technology of Taiwan under Grant MOST 106-2221-E-035-054-MY3. Recommended for publication by Associate Editor X. Luo upon evaluation of reviewers' comments. (*Corresponding author: Chingfu Tsou.*)

Chengshiu Liou is with the Ph.D. Program of Electrical and Communications Engineering, Feng Chia University, Taichung 40724, Taiwan (e-mail: asdf008844@gmail.com).

Fuchi Shih, Yuanyuan Huang, Zihong Hu, and Chingfu Tsou are with the Department of Automatic Control Engineering, Feng Chia University, Taichung 40724, Taiwan (e-mail: cftsou@fcu.edu.tw).

Weileun Fang is with the Institute of NanoEngineering and MicroSystems, National Tsing Hua University, Hsinchu 30013, Taiwan, and also with the Department of Power Mechanical Engineering, National Tsing Hua University, Hsinchu 30013, Taiwan (e-mail: fang@pme.nthu.edu.tw).

Color versions of one or more figures in this article are available at <https://doi.org/10.1109/TCPMT.2021.3049563>.

Digital Object Identifier 10.1109/TCPMT.2021.3049563

In an earlier study, the reflector was widely assembled with the mini- or micro-LED devices to realize high-resolution display panel [10]–[12]. Also, different taper angles on the microreflector were designed and evaluated to integrate with micro-LED array [13]. For optogenetics, the microreflector was used to enhance the micro-LED based light source [14]. This can successfully resolve the issue of the diverged light source, and greatly increase the optical performance of the display. Utilizing bulk micromachining technology, the reflectors can be fabricated at a low cost and with precision in batch production. Unfortunately, these assembly approaches involve some problems. The large size of the reflector and the precise alignment requirement make this approach difficult to apply for the micro-LED display. On the other hand, when the reflective material was coated around the GaN etching structure to collect the leakage emitting rays from a sidewall, it improved the optical performance of micro-LED array, in which we have the 42% of the maximum increase [15]–[17]. Based on the efficiency improvement by GaN-based microreflector, the sapphire substrate, fabricated with the optic, can provide an extended reflective surface to further improve the performance and reduce the optical crosstalk. The sapphire structure with an optical design has potential for application in the micro-LED display; particularly, the sapphire substrate is usually used for LED epi-wafer as well as the micro-LED arrays. Based on mature sapphire etching technology, the sapphire shaping structure can form directly on the intrinsic structure of the LED die. Assisted with the maskless pattern approach, sapphire nanopylramids were fabricated to improve the quality of GaN growth and reduce the total internal reflection (TIR); consequently, the output performance was remarkably enhanced [18]. Fabricated in a cylinder structure array on the double side of a sapphire substrate, the cyclical profile can reduce the TIR effect and improve LED lighting performance, compared with a flat surface [19]. Therefore, these approaches can not only improve the optical performance but also meet the compact size requirements of a micro-LED device.

As described in previous works, though the micro-LED display can be realized by the microfabrication process, the optical performance for this emerging display technology can still be improved. Therefore, based on the mature sapphire etching technology in the conventional LED industry, this article proposed a new design for the micro-LED array with a sapphire microreflector. It aimed to reduce the optical crosstalk between neighboring pixels and increase efficiency for the micro-LED array. It evaluated the sapphire microreflector with different thicknesses using TracePro, a commercial software. To confirm the design concept, this research carried out the micro-LED fabrication process by integrating it with the sapphire etching technology. After that, the micro-LED array with sapphire micro-reflector and with common-N interconnection was completed, respectively. Finally, their optical characteristics were compared and verified.

## II. DESIGN AND SIMULATION

The inductively coupled plasma (ICP) etching and photolithograph technology were employed in this study; the

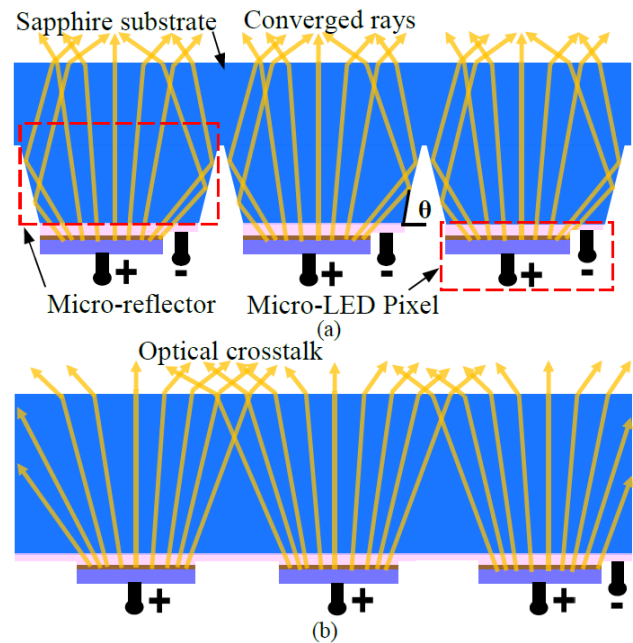


Fig. 1. Emitting rays in the micro-LED arrays. (a) Proposed micro-LED array with concentration of ray distribution. (b) Typical common-N micro-LED array with wide divergence of ray distribution.

parameters for the fabrication process were adopted from previous work [20]. It was an efficient way for the optic structure to be directly formed with each micro-LED pixel. As shown in Fig. 1(a), the proposed array contains micro-LED pixels, individual electrodes, a sapphire microreflector and a sapphire substrate. In addition, the pixel size of the micro-LED pixel is  $75 \mu\text{m}$ , with a center-to-center pitch of  $85 \mu\text{m}$ . During the etching process, the etching trench forms on the sapphire substrate so as to directly fabricate microreflectors. They may have different inclination angles ( $\theta$ ), from  $65^\circ$  to  $90^\circ$ , on the sapphire structure because of the etching conditions, such as gas combination, the density of BCl radicals in plasma, D. C bias power [21], [22]. In particular, the  $90^\circ$  of inclination angle can meet the requirement for high-resolution displays; therefore, the angle was set as the ideal case in simulation. Compared with the conventional micro-LED array, as shown in Fig. 1(b), the sapphire microreflector can realize light intensity concentration, in accordance with Snell's law; as a result, the optical crosstalk between adjacent micro-LED pixels is suppressed. On the other hand, it is worth mentioning that each micro-LED pixel on the proposed array owns a pair of electrodes to themselves and the etching trench isolates the interconnection between pixels. This is different from the conventional micro-LED array which shares electrodes with a common-N cathode. In the intrinsic structure of the epi-layer, the anodes (marked with +) are defined on the P-GaN layer, and then the cathodes (marked with -) are fabricated on the N-GaN layer by the etching part of the epi-layer. Obviously, the interconnection for the proposed micro-LED array does not share an N-GaN layer, which means that the conductive path of different series resistance is removed. Theoretically, each emitting micro-LED pixel has nearly consistent impedance. Moreover, with the design of individually controllable

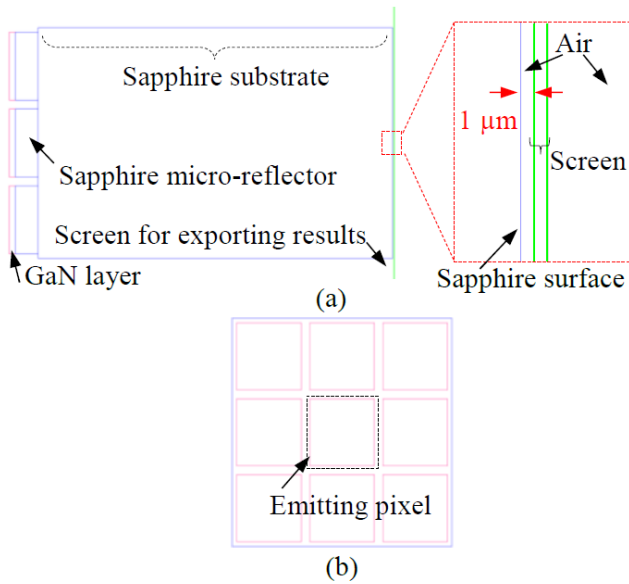


Fig. 2. (a) Established simulation model of micro-LED arrays. (b) Simplified model with 3 × 3 matrix of micro-LED pixels.

TABLE I

FEATURE SIZE AND PROPERTY SETTING OF SIMULATION MODEL

Thickness of structure					
GaN layer (μm)	7				
Micro-reflector, d (μm)	5	10	15	20	25
Properties of model					
Refractive index	2.68 / 1.62 (GaN / Sapphire)				
Luminous flux (lm)	15.4				
Light ray (count)	100,000				

electrodes, the proposed micro-LED array is compatible with an active matrix (AM) circuit or a passive matrix (PM) circuit. Utilizing the flip-chip technology, the proposed array can bond with a control circuit to accomplish the display module with high resolution.

Following the design concept, the commercial software, TracePro, was utilized for optical simulation. The typical model of the proposed micro-LED arrays is shown in Fig. 2(a), which includes the GaN structure and sapphire substrate with microreflector. To understand the optical mechanism, models with different feature sizes were built and set with the corresponding parameters as shown in Table I. Besides, the thickness of the total sapphire part, including the sapphire substrate and the sapphire microreflector, was set to 418 μm. With structure geometry of trigonometry, the maximum etching depth was evaluated as 25 μm because the hard mask with 80° inclination angle on the structure profile limited the sapphire etching angle on the V-trench, which was extracted by the previous experiment. The inclination angle on the sapphire microreflector was fixed at 90° for an ideal case and the model’s surrounding was usually air. To evaluate the light intensity distribution, a 1 mm × 1 mm screen used to accept the rays. In addition, there was a 1-μm view distance between the screen and bottom surface of the sapphire substrate. As shown in Fig. 2(b), the simplified model with 3 × 3 matrix of micro-LED pixels was used to simplify

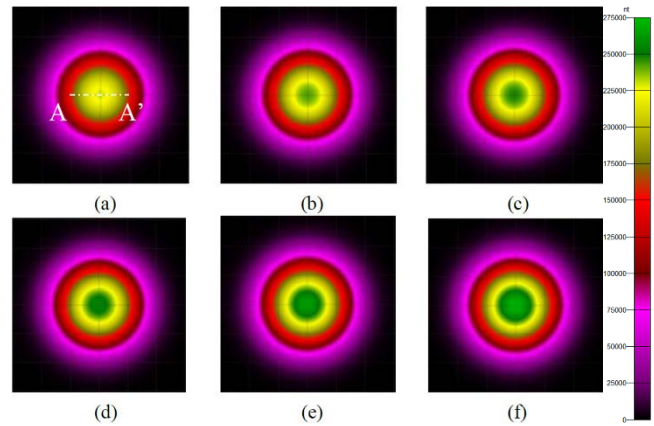


Fig. 3. Simulated light intensity pattern for micro-LED arrays with different sapphire microreflector thicknesses. (a) Common-N (reference array). (b) 5 μm. (c) 10 μm. (d) 15 μm. (e) 20 μm. (f) 25 μm.

the simulation process and save memory usage. In addition, the model with common-N interconnection, which had only 2 μm of etching depth on the GaN layer, was also built as a reference array. Utilizing the Monte Carlo ray-tracing method and Snell’s law, most of the emitting rays from the center of the pixels sequentially went through the GaN structure, bulk sapphire and air, and finally arrived at the screen with 600 μm × 600 μm area. As shown in Fig. 3, it was obvious that the microreflector effectively concentrated the light intensity, compared with the reference array. The thickness of the sapphire microreflector increased from 5 to 25 μm, and then the light intensity pattern at the green part (the color corresponded with the light intensity from 227 500 to 275 000 nt) was increased from 85 to 154 μm in diameter, as shown in Fig. 3(b)–(f). On the contrary, the light intensity pattern at the green part, emitting from the reference array, was only 23 μm in diameter, as shown in Fig. 3(a). After that, the light intensity distributions on the corresponding patterns were traced along A-A’ line with a length of 250 μm. As shown in Fig. 4, the microreflector effectively concentrated the light intensity, compared with the reference array. With the increasing thickness of the sapphire microreflector from 5 to 25 μm, light intensity was remarkably increased at the top position of the emitting pixel (the position from -42.5 to 42.5 μm). On the contrary, the increase in light intensity was relatively low at positions from 42.5 to 125 μm and -42.5 to -125 μm.

To quantitatively evaluate the findings, light intensity distributions at the top region of emitting pixels were averaged and sequentially normalized, and then the results were summarized in Fig. 5. Compared with the reference array, the normalized light intensity at the top position of the emitting pixel was obviously raised from 0.84 to 0.89 when the sapphire microreflector with 5 μm of thickness was used. In addition, the normalized light intensity at the top position of the adjacent pixel increased from 0.63 to 0.67. With increasing thickness of the sapphire microreflector from 5 to 25 μm, the normalized light intensity at the top position of the central pixel and adjacent pixel increased from 0.89 to 1 and from 0.67 to 0.76, respectively. Though the contrasts on the adjacent pixel were

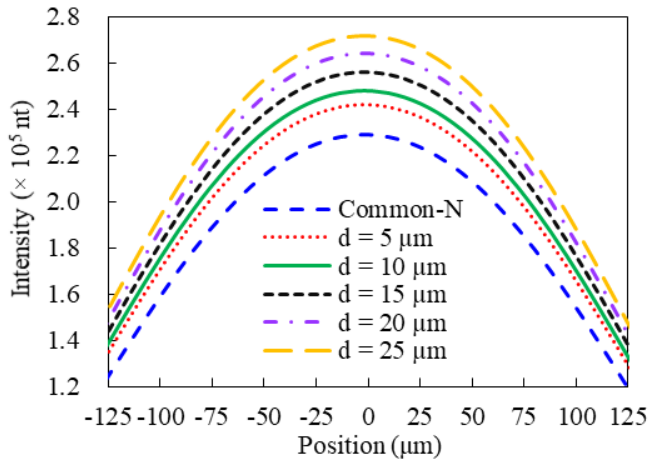


Fig. 4. Simulated light intensity distribution with different sapphire micro-reflector thicknesses along A-A' line.

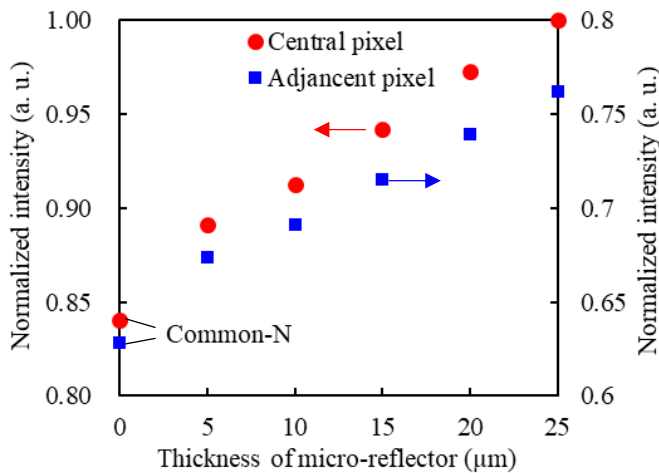


Fig. 5. Simulated light intensity distribution with different sapphire micro-reflector thicknesses.

all about 1 for different thicknesses, it is obvious that the light intensity increase on the central pixel has a steeper slope compared with the increase in the adjacent pixel; therefore, the contrast was improved. The results show that a thicker sapphire microreflector can improve the efficiency of a micro-LED array because the area of the reflective surface increased, which caused more rays to be effectively reflected. Particularly, the light intensity had a 20% maximum increase against the reference array. Theoretically, more emitting rays were collected on the desired area and less emitting rays distributed in the structure of the micro-LED array, which means contrast on the array could be also increased.

### III. EXPERIMENT AND DISCUSSION

#### A. Microfabrication

To confirm the design concept of the microreflector, and application to the micro-LED array, the typical arrays were fabricated by a microfabrication process. During the photolithography process, two masks were used for sapphire etching and GaN mesa etching, respectively; these provided precise patterning alignment. The ICP etching technology was the key process in the realization of the microreflector formed with the micro-LED pixel. In the etching steps, the GaN and

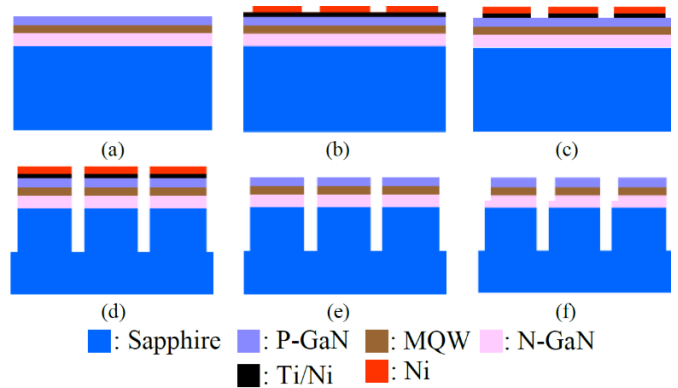


Fig. 6. Fabrication process of the proposed micro-LED array. (a) LED epi-wafer. (b) Ti/Ni deposition, and then hard mask patterning and deposition. (c) Etching window opening. (d) GaN and sapphire ICP etching. (e) Hard mask removed. (f) GaN mesa etching.

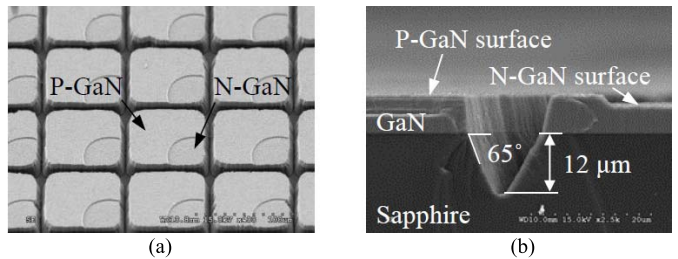


Fig. 7. (a) Accomplished micro-LED array with sapphire microreflector. (b) Sapphire microreflector with specific inclination angle.

sapphire were sequentially etched. The fabrication process flow of the proposed micro-LED array was shown in Fig. 6 and the details described as follows. First, the commercial epi-wafer was used as the substrate, which is GaN-based and at blue light wavelength, depicted in Fig. 6(a). After that, the seed layer, composed of dual layers with Ti/Ni (5 nm/50 nm), was deposited by an E-Gun evaporator. Subsequently, the patterned hard mask, about 19- $\mu$ m thickness, was defined by photolithography and formed by the Ni electroplating process, as shown in Fig. 6(b). To open the etching window, the exposure part of the seed layer were sequentially removed by 30% of nitric acid (HNO<sub>3</sub>) solution and commercial buffered oxide etchant (BOE), depicted in Fig. 6(c). During the ICP etching process, GaN and sapphire were etched, as depicted in Fig. 6(d). After that, the residual hard mask was sequentially removed by 30% of the nitric acid solution and BOE, depicted in Fig. 6(e). Finally, the Cl<sub>2</sub>-based ICP etching was used again for the N-GaN layer exposure, depicted in Fig. 6(f). Besides, on the other epi-wafer, the reference array with a common-N interconnection was also fabricated at the GaN etching step, in which, to simplify the process, the 6  $\mu$ m thickness of the photoresist pattern replaced the Ni-hard mask as the etching mask. To reduce the structural change of the photoresist pattern, hard bake was carried on a hot plate at 90° in 1 day.

The proposed micro-LED array with 16  $\times$  16 matrix was successfully completed, as shown in Fig. 7(a). The top view of each micro-LED pixel had a size of 73  $\mu$ m  $\times$  73  $\mu$ m on a pitch of 85  $\mu$ m and 300-dpi resolution. Surrounding each micro-LED pixel, the V-shaped trench with a 12- $\mu$ m gap provided electrical isolation. The photolithography

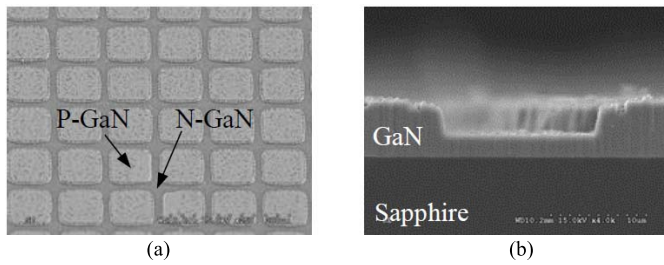


Fig. 8. (a) Accomplished micro-LED array with common-N interconnection. (b) Exposure N-GaN part after GaN etching.

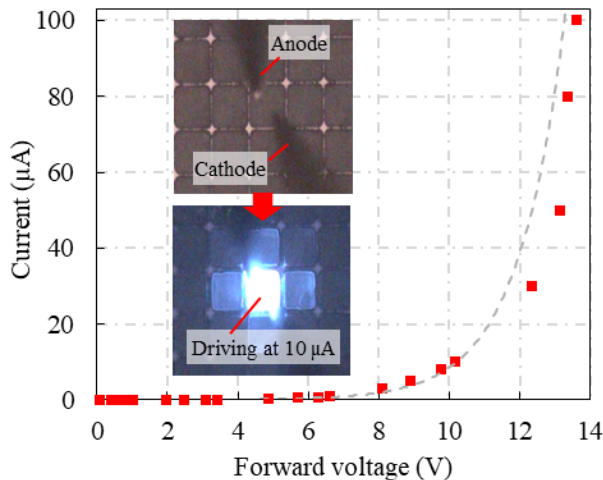


Fig. 9. Current–voltage ( $I - V$ ) characteristic of the micro-LED pixel with sapphire microreflector and the operating condition.

process caused little lateral shrinkage of  $2\text{-}\mu\text{m}$  linewidth loss on the micro-LED pixel. After mesa etching, which relied on the ICP etching technology, the individual electrode on each micro-LED pixel was clearly defined. The N-GaN layer was exposed with a quarter circle pattern and this served as cathode; the etching depth was about  $2\ \mu\text{m}$ . Meanwhile, the nonetching area served as the anode with the P-GaN surface. Following the GaN and sapphire etching processes, the sapphire shaping structure was directly formed on each micro-LED pixel and functioned as the microreflector, as shown in Fig. 7(b). Because of the microlading effect, the maximum etching depth and inclination angle on the sapphire microreflector were  $12\ \mu\text{m}$  and  $65^\circ$ , respectively. The micro-LED array with common-N interconnection was also fulfilled as a reference array, as shown in Fig. 8(a), and the trench surrounding each micro-LED pixel served as a common cathode; the etching depth was  $3\ \mu\text{m}$ , as shown in Fig. 8(b). Besides, the reference array has a linewidth loss of about  $5\ \mu\text{m}$  because the photoresist (AZ4620) had little change during the  $\text{Cl}_2$ -based ICP etching process. The sidewall roughness on the GaN surface and the sapphire surface are  $R_a = 39\ \text{nm}$  and  $R_a = 47\ \text{nm}$ , respectively, which were measured by the Atomic Force Microscopy (AFM) system. As shown in the fabrication results, the structure profile had a slight difference, compared with the ideal design, which would be analyzed.

To operate the proposed micro-LED array, the current–voltage ( $I - V$ ) characteristic was measured, as shown in Fig. 9 with a fitting line (gray dotted line). First, the probe station

and micro-LED array were fixed tight on the measurement platform with a backside observation window. After that, the CCD-based camera, assisted with a microscope, focused on the GaN side to correct the corresponding position between tungsten microprobes ( $5\text{-}\mu\text{m}$  tip diameter) and electrodes on the micro-LED pixel. During the measurement, a pixel was driving with constant current from  $1\ \text{nA}$  to  $110\ \mu\text{A}$ , and the standard deviation of the corresponding voltage was less than  $0.5\ \text{V}$ . In addition, the forward voltage was defined as  $11.8 \pm 0.4\ \text{V}$ , according to the tangent method [23], and the micro-LED pixels broke at  $110\ \mu\text{A}$ . The measurement results show that the proposed micro-LED unit with individual electrodes had good electrical uniformity. On the other hand, there have rays emitting from the side wall of the GaN layer when driving a micro-LED pixel, and then the surrounding structure of micro-LEDs was illuminated. Theoretically, the reflected rays on the GaN side were in opposite direction to the sapphire surface, therefore the influence on the backside of that sapphire substrate was slight.

### B. Optical Characteristic

The electrical interconnection between the contact resistance (between microprobe and P-GaN surface), path resistance, and micro-LED pixel was in series [6], [24]. Theoretically, when a constant current is applied on a pixel at the proposed and reference micro-LED array, the same current would pass through, respectively; therefore, the micro-LED pixels would drive with nearly similar power. Consequently,  $10\ \mu\text{A}$  of the constant current was supplied in the following experiment. In the experiment, the camera was focused on the backside of the sapphire substrate to capture the light intensity distribution from fulfilled micro-LED arrays. Besides, there was only air between the camera and sapphire surface, and the experiment was carried out in a dark room. This method was implemented in studies of micro-LED application, such as biological imaging and inspection of micro-LED arrays [25]–[27]. Based on the image sensor, the camera can accept the emitted rays, and then it converts the optical signal in vision wavelength to the voltage signal. Following the digitization process, the image is the digital layout for the pixel value. Therefore, the pixel value highly depends on the light intensity from the captured target.

In the measurement, the camera was first tested to avoid insufficient and excessive exposure when the micro-LED unit was driving. Then, the parameters of the camera were set as  $1/100\ \text{s}$  of exposure time,  $f/2.8$   $f$ -number, and  $6\text{-mm}$  focal length. On the proposed and reference micro-LED arrays, the single-pixel was driving, respectively, and then the corresponding light intensity patterns were obtained, as shown in Fig. 10. In Fig. 10(a), more light intensity was observed in the central area, as compared with the pattern shown in Fig. 10(b). For quantitative comparison, their normalized light intensity distributions were traced along B-B' line, which included 11 micro-LED pixels and was exported by an image processing program (ImageJ), as shown in Fig. 11. In addition, the emitting pixel was at the central position. The results revealed that the sidewall of the microreflector could reflect

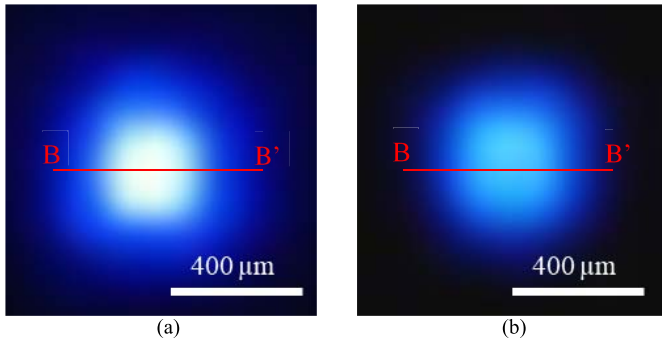


Fig. 10. Captured light intensity patterns of micro-LED arrays. (a) With sapphire microreflector. (b) With common-N interconnection.

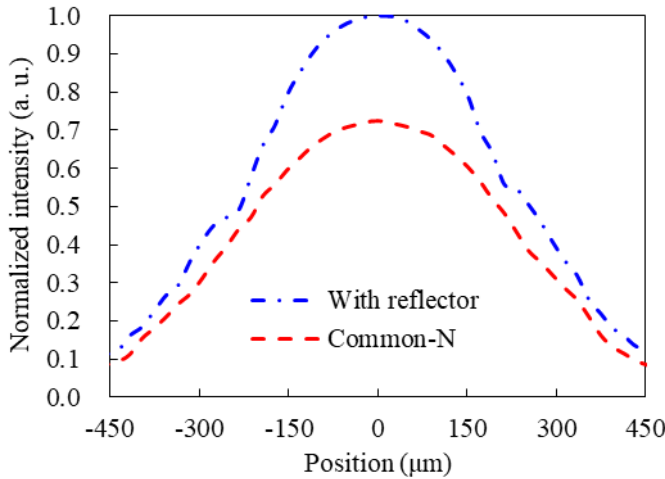


Fig. 11. Experimented normalized light intensity distributions along B-B' line.

the mostly diverged light rays; therefore, there was the light intensity increased 37% at a position from  $-42.5$  to  $42.5 \mu\text{m}$ . Moreover, the contrast between the adjacent pixel, at the position from  $-127.5$  to  $-42.5 \mu\text{m}$  and  $42.5$  to  $127.5 \mu\text{m}$ , and central pixel was 1 for both fulfilled micro-LED arrays. At the position from  $-382.5$  to  $-467.5 \mu\text{m}$  and  $382.5$  to  $467.5 \mu\text{m}$ , the contrasts were 8 and 14 for the reference array and the micro-LED array with microreflector, respectively. Consequently, compared with the conventional design of a monolithic micro-LED array with common-N interconnection, the sapphire microreflector not only improved the optical efficiency but also increased the contrast on the micro-LED array, which is beneficial for display application.

The sapphire microreflector with  $65^\circ$  specific inclination angle was completed on the proposed micro-LED array; this was different from the ideal case in Section II. To analyze the optical influence of the difference, TracePro was used. The property setting was the same as that in Table I and the simulation model was similar to the architecture shown in Fig. 2. First, the difference in pixel size between the design of the ideal case and the measurement result was evaluated, and then the results indicated that the influence of the different pixel sizes could be ignored. Therefore, the pixel sizes of the fulfilled micro-LED arrays were imported in the latter analysis. To determine the difference between the ideal with  $90^\circ$  of inclination angle and fulfilled micro-LED array, the measured

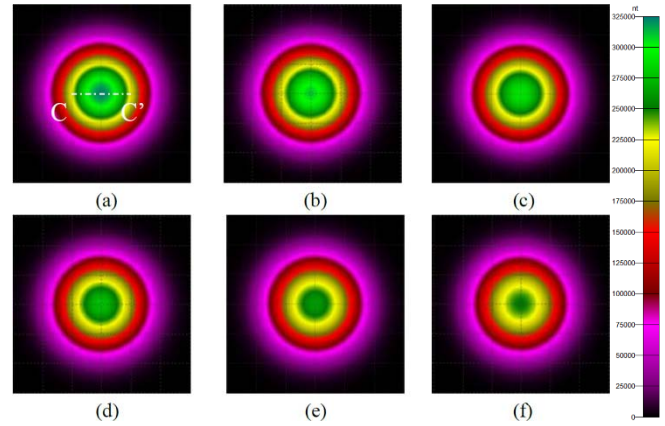


Fig. 12. Simulated light intensity pattern for sapphire microreflectors with different inclination angles. (a)  $65^\circ$ . (b)  $70^\circ$ . (c)  $75^\circ$ . (d)  $80^\circ$ . (e)  $85^\circ$ . (f)  $90^\circ$ .

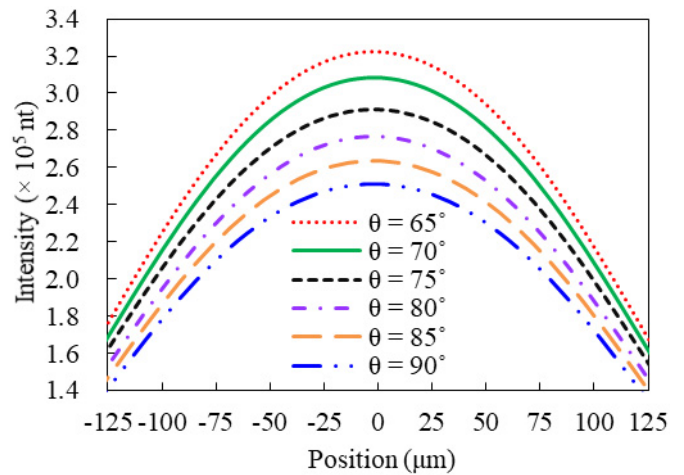


Fig. 13. Analyzed light intensity distributions with different inclination angles along C-C' line.

result of etching depth and the gap were considered as the boundary condition for the following analysis. Hence, as shown in Fig. 7, when the etching depth of the sapphire is  $12 \mu\text{m}$ , the minimum inclination angle was limited to  $65^\circ$ . Subsequently, the influence of a variety of inclination angles ( $65^\circ$ ,  $70^\circ$ ,  $75^\circ$ ,  $80^\circ$ ,  $85^\circ$ , and  $90^\circ$ ) on the sapphire microreflector was analyzed. The corresponding light intensity patterns are shown in Fig. 12. Obviously, there were significant improvements, for example, the emitting rays concentrated in the diameter of the green part (the color corresponded with light intensity from 227 500 to 325 000 nt) was increased from 93 to  $179 \mu\text{m}$  diameters, as shown in Fig. 12(a)–(f). The light intensity distribution was then further be traced along the C-C' line, as shown in Fig. 13. Compared with the ideal  $90^\circ$  inclination angle, the light intensity had remarkably increased at  $65^\circ$  inclination angle, especially from  $-42.5$  to  $42.5 \mu\text{m}$ . To further explain the improvement of the inclination angle, the light intensity distributions for each case were carried on the normalization approach; this approach was similarly used for the summarization in Fig. 5. After that, the results were summarized in Fig. 14. With the decreasing inclination angle of the sapphire microreflector from  $90^\circ$  to  $65^\circ$ , the normalized light intensity on the top position of the central pixel and

TABLE II  
SUMMARIZED CONTRAST ON DIFFERENT PIXELS FOR SIMULATION, EXPERIMENT, AND ANALYSIS

Case	A (Simulation)	B (Simulation)	C (Simulation)	D (Analysis)	E (Analysis)	F (Analysis)	Common-N (Experiment)	With reflector (Experiment)	
Thickness for reflector ( $\mu\text{m}$ )	0 (Reference)	12	15	0 (Reference)	12	12	0	12	
Inclination angle on reflector	Non	90°	90°	Non	90°	65°	Non	65°	
Contrast	$I_0/I_5$	25	39	42	25	40	55	8	14
	$I_0/I_4$	4	5	5	4	5	7	3	5
	$I_0/I_3$	2	2	2	2	2	2	2	2
	$I_0/I_2$	1							
	$I_0/I_1$	1							
	$I_0/I_0$	1 (Emitting pixel)							
Schematic diagram for contrast evaluation									
	<p><math>P_0</math>: Central emitting pixel  <math>P_n</math>: Neighboring pixel  <math>I_n</math>: Light intensity on corresponding pixel</p> <p><math>I_0</math>: Light intensity on central pixel  <math>n</math>: Ordinal number for neighboring pixels</p>								

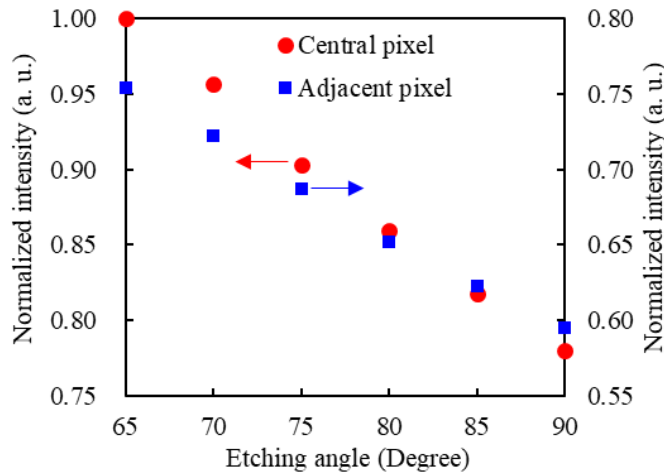


Fig. 14. Analyzed normalization light intensity with different inclination angles on sapphire microreflectors.

adjacent pixel increased from 0.78 to 1 and from 0.6 to 0.75, respectively. It is worth noting that the light intensity increase on the central pixel has a steeper slope than that on the adjacent pixel; specifically, it had 28% maximum increase at 65° inclination angle. According to the results shown in Fig. 5, micro-LED array with the 65° inclination angle had a 41% maximum increase of the light intensity, compared with the reference array, which was in good agreement with the measurement results. Therefore, the inclination angle on the sapphire microreflector can further improve the performance of the micro-LED array. On the other hand, an optimal inclination angle for the microreflector can be determined by the etching parameters and the design of the etching window.

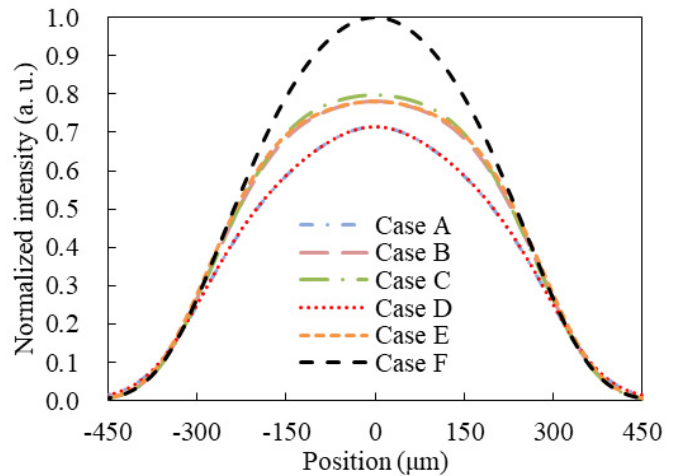


Fig. 15. Analyzed and simulated normalized light intensity distribution for different cases with 11 × 11 matrix of micro-LEDs.

In order to determine the contrast improvement on the neighboring pixels, some simulated and analyzed models in the forward part were extended to 11 × 11 matrix of micro-LED pixels and evaluated. The results were compared with the experimental results to further verify the improvement of the fulfilled micro-LED array. The normalized light intensity distributions for different cases are summarized in Fig. 15 and the corresponding features are shown in Table II. The problems on fabrication imperfection on the fulfilled micro-LED arrays were discussed. The linewidth losses on the micro-LED array with sapphire microreflector and reference array were about 2 and 5  $\mu\text{m}$ , respectively. These slightly affected the optical performance because the light intensity distributions and contrast of neighboring pixels matched, such as Case A

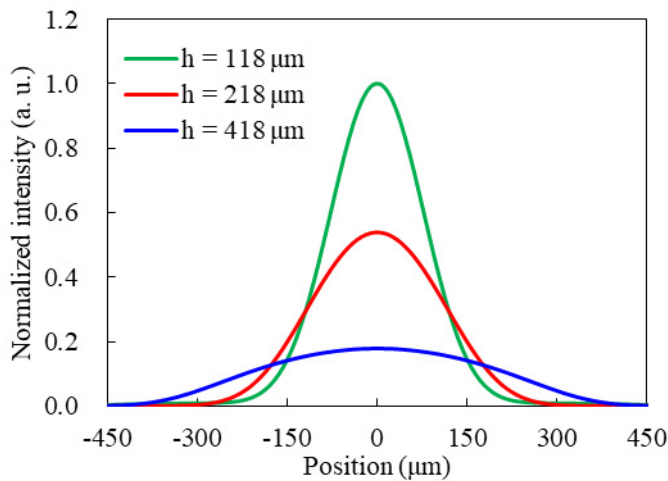


Fig. 16. Analyzed light intensity distribution for different sapphire substrate thicknesses.

matched Case D and Case B matched Case E. In addition, the difference of etching depths on the micro-LED structure was also influenced slightly, comparing Case B and Case C.

On the other hand, the normalized light intensities ( $I_0 - I_5$ ) with the corresponding position of pixels ( $P_0 - P_5$ ) would be evaluated to further calculate the contrast on the micro-LED array. As shown in Fig. 15, the sapphire microreflector could effectively concentrate the emitting rays as indicated by the increased light intensity distribution in the central area near the emitting pixel ( $P_0$ ). The contrasts of near pixels ( $P_1$  and  $P_2$ ) were improved indeed because the intensity difference increased with thicker microreflector and lower inclination angle, based on the discussion of the Figs. 5 and 14. Moreover, the contrast started to increase at  $P_3 - P_5$  due to the increasing light intensity in the central area (Top of  $P_0 - P_2$ ) with reducing light intensity at the neighboring area (top of  $P_3 - P_5$ ), which was the function of the sapphire microreflector. Particularly, there was a great increase on top of  $P_5$  area for the cases with sapphire microreflector, in which the  $65^\circ$  of inclination angle had the best improvement with 55 of contrast, as shown in Table II at Case F. Therefore, the optical crosstalk was suppressed between the pixels. Although the rough sidewall on fulfilled micro-LED arrays caused diffuse reflection, the contrast and performance of the micro-LED array were still improved by the proposed design concept, verified in experiment and analysis results. In the central area (top of  $P_0 - P_3$ ) for Case D, Case F and experiment results, the light intensity profiles and contrasts matched, respectively, as shown in Table II, Figs. 11 and 15. Compared with the reference array, the  $65^\circ$  inclination angle on microreflector had a maximum intensity increase of 37% in the experiment and 41% in the analysis; therefore, most of the light rays were concentrated in the desired area on a fulfilled array with microreflector. The difference between Figs. 11 and 15 suggests that fewer diffused rays, reflected from rough sidewall, caused in an increase of normalized light intensity on the background and a reduction of the contrast.

On the other hand, the sidewall roughness on GaN surface and sapphire microreflector can improve by gas combination

of etching process [28]–[30]. Then, the diffused reflection can be greatly reduced and the contrast on the micro-LED array increased. Additionally, the chemical–mechanical planarization (CMP) process has been widely used in the LED industry to reduce the thickness of sapphire substrate; therefore, the contrast of micro-LED array with sapphire microreflector can be further increased. As shown in Fig. 16, thinner sapphire substrates have better improvement. In particular, the contrasts on top of  $P_5$ ,  $P_2$ , and  $P_1$  can be 440, 10, and 2, respectively, when the thickness of the sapphire substrate is  $100 \mu\text{m}$ .

#### IV. CONCLUSION

This study successfully fabricated the micro-LED array with the sapphire microreflector. The array had  $16 \times 16$  matrix,  $85\text{-}\mu\text{m}$  pitch, and a 300-dpi resolution. Utilizing the commercial simulation program (TracePro), the optical mechanism of the micro-LED arrays was verified. The simulation results show that the sapphire microreflector with  $25 \mu\text{m}$  thickness has a 20% improvement in light intensity and improve the contrast between the adjacent pixels, compared with the reference array. Due to the larger area of reflective surface, more rays were reflected at the top region of the emitting pixel. Therefore, the deeper etching depth was beneficial for the performance of the micro-LED array. Based on the extracted etching parameters, the micro-LED fabrication process, which is integrated with the sapphire deep etching process was carried out. Due to the microloading effect, the maximum etching depth and specific inclination angle of the sapphire shaping structure were  $12 \mu\text{m}$  and  $65^\circ$ , respectively. Experimental results show that the sapphire microreflector improved by 37% in light intensity at the corresponding area of the emitting pixel, as compared with the reference array. Therefore, the rays distributed on the undesired area were significantly decreased, and the contrast of the nearing pixel was increased compared with the reference array and the optical crosstalk was also suppressed. Moreover, the rough surface on the microreflector can be optimized by the ICP etching process, and the contrast on the micro-LED array can further increase. On the other hand, the results also indicate that the inclination angle on the sapphire microreflector could further optimize the optical performance. Therefore, this approach was verified as beneficial for application to micro-LED display.

#### ACKNOWLEDGMENT

The authors would like to thank the Precision Instrument Support Center of Feng Chia University, Nano Facility Center of National Chiao Tung University and Taiwan Semiconductor Research Institute (TSRI) in providing the fabrication facilities.

#### REFERENCES

- [1] C.H. Chiu *et al.*, “Metal organic chemical vapor deposition growth of GaN-based light emitting diodes with naturally formed nano pyramids,” *Jpn. J. Appl. Phys.*, vol. 47, no. 4, pp. 2954–2956, Apr. 2008.
- [2] S. Che, A. Yuki, H. Watanabe, Y. Ishitani, and A. Yoshikawa, “Fabrication of asymmetric GaN/InN/InGaN/GaN quantum-well light emitting diodes for reducing the quantum-confined stark effect in the blue-green region,” *Appl. Phys. Exp.*, vol. 2, Jan. 2009, Art. no. 021001.

- [3] C. X. Ren *et al.*, "Analysis of defect-related inhomogeneous electroluminescence in InGaN/GaN QW LEDs," *Superlattices Microstructures*, vol. 99, pp. 118–124, Nov. 2016.
- [4] H. H. Hu, K. K. C. Chang, and A. Bible, "Micro device with stabilization post," U.S. Patent 9035 279 B2, May 19, 2015.
- [5] Z. J. Liu, W. C. Chong, K. M. Wong, and K. M. Lau, "360 PPI flip-chip mounted active matrix addressable light emitting diode on silicon (LEDoS) micro-displays," *J. Display Technol.*, vol. 9, no. 8, pp. 678–682, Aug. 2013.
- [6] Z. Gong *et al.*, "Matrix-addressable micropixelated InGaN light-emitting diodes with uniform emission and increased light output," *IEEE Trans. Electron Devices*, vol. 54, no. 10, pp. 2650–2658, Oct. 2007.
- [7] C. M. Kang *et al.*, "Fabrication of a vertically-stacked passive-matrix micro-LED array structure for a dual color display," *Opt. Exp.*, vol. 25, no. 3, pp. 2489–2495, Feb. 2017.
- [8] H. V. Han *et al.*, "Resonant-enhanced full-color emission of quantum-dot-based micro LED display technology," *Opt. Exp.*, vol. 23, no. 25, pp. 32504–32515, Dec. 2015.
- [9] H. Y. Lin *et al.*, "Optical cross-talk reduction in a quantum-dot-based full-color micro-light-emitting-diode display by a lithographic-fabricated photoresist mold," *Photon. Res.*, vol. 5, no. 5, pp. 411–416, Oct. 2017.
- [10] K. Takahashi, S. Nakajima, and S. Takeuchi, "Full color LED display panel fabricated on a silicon microreflector," in *Proc. IEEE 10th Annu. Int. Workshop Micro Electro Mech. Syst. Invest. Micro Struct., Sensors, Actuat., Mach. Robots*, Nagoya, Japan, Jun. 1997, pp. 356–362.
- [11] C. T. Tsou and Y.-S. Huang, "Silicon-based packaging platform for light-emitting diode," *IEEE Trans. Adv. Packag.*, vol. 29, no. 3, pp. 607–614, Aug. 2006.
- [12] Y. J. Jiaying, F. Ou, W. C. Chong, L. Zhang, and Q. M. Li, "Micro display panels with integrated micro-reflectors," U.S. Patent 10 304 375 B2, May 28, 2019.
- [13] F. Gou, E.-L. Hsiang, G. Tan, Y.-F. Lan, C.-Y. Tsai, and S.-T. Wu, "Tripling the optical efficiency of color-converted micro-LED displays with funnel-tube array," *Crystals*, vol. 9, no. 1, p. 39, Jan. 2019.
- [14] W. Khan, M. Setien, E. Purcell, and W. Li, "Micro-reflector integrated multichannel  $\mu$ LED optogenetic neurostimulator with enhanced intensity," *Frontiers Mech. Eng.*, vol. 4, p. 00017, Nov. 2018.
- [15] P.-W. Chen *et al.*, "Improved performance of passive-matrix micro-LED displays using a multi-function passivation structure," *IEEE Photon. J.*, vol. 12, no. 4, Jun. 2020, Art. no. 7000711.
- [16] K. Bulashevich, S. Konoplev, and S. Karpov, "Effect of die shape and size on performance of III-nitride micro-LEDs: A modeling study," *Photonics*, vol. 5, no. 4, p. 41, Oct. 2018.
- [17] W. Guo, H. Meng, Y. Chen, T. Sun, and Y. Li, "Wafer-level monolithic integration of vertical micro-LEDs on glass," *IEEE Photon. Technol. Lett.*, vol. 32, no. 12, pp. 673–676, Jun. 15, 2020.
- [18] H. Gao, F. Yan, Y. Zhang, J. Li, Y. Zeng, and G. Wang, "Fabrication of nano-patterned sapphire substrates and their application to the improvement of the performance of GaN-based LEDs," *J. Phys. D, Appl. Phys.*, vol. 41, no. 11, May 2008, Art. no. 115106.
- [19] C. F. Shen, S. J. Chang, W. S. Chen, T. K. Ko, C. T. Kuo, and S. C. Shei, "Nitride-based high-power flip-chip LED with double-side patterned sapphire substrate," *IEEE Photon. Technol. Lett.*, vol. 19, no. 10, pp. 780–782, May 15, 2007.
- [20] C. Liou *et al.*, "Design and fabrication of micro-LED display with sapphire micro-reflector array," in *Proc. IEEE Int. Conf. Micro Electro Mech. Syst. (MEMS)*, Vancouver, BC, Canada, Jan. 2020, pp. 1153–1156.
- [21] C. H. Jeong, D. W. Kim, K. N. Kim, and G. Y. Yeom, "Sapphire etching with  $\text{BCl}_3/\text{HBr}/\text{Ar}$  plasma," *Jpn. J. Appl. Phys.*, vol. 171, nos. 1–3, pp. 280–284, Jul. 2003.
- [22] P.-C. Chen *et al.*, "Bulk vertical micromachining of single-crystal sapphire using inductively coupled plasma etching for X-ray resonant cavities," *J. Micromech. Microeng.*, vol. 25, no. 1, Jan. 2015, Art. no. 015016.
- [23] B. Guilhabert *et al.*, "Sub-micron lithography using InGaN micro-LEDs: Mask-free fabrication of LED arrays," *IEEE Photon. Technol. Lett.*, vol. 24, no. 24, pp. 2221–2224, Dec. 15, 2012.
- [24] R.-H. Horng, H.-Y. Chien, F.-G. Tarntair, and D.-S. Wu, "Fabrication and study on red light micro-LED displays," *IEEE J. Electron Devices Soc.*, vol. 6, pp. 1064–1069, Aug. 2018.
- [25] L. Zheng *et al.*, "Research on a camera-based microscopic imaging system to inspect the surface luminance of the micro-LED array," *IEEE Access*, vol. 6, pp. 51329–51336, Sep. 2018.
- [26] N. Grossman *et al.*, "Multi-site optical excitation using  $\text{ChR}_2$  and micro-LED array," *J. Neural Eng.*, vol. 7, no. 1, Feb. 2010, Art. no. 016004.
- [27] A. Nakajima *et al.*, "CMOS image sensor integrated with micro-LED and multielectrode arrays for the patterned photostimulation and multichannel recording of neuronal tissue," *Opt. Exp.*, vol. 20, no. 6, pp. 6097–6108, Feb. 2012.
- [28] Y. P. Hsu *et al.*, "ICP etching of sapphire substrates," *Opt. Mater.*, vol. 27, no. 6, pp. 1171–1174, Mar. 2005.
- [29] D. S. Rawal, B. K. Sehgal, R. Muralidharan, H. K. Malik, and A. Dasgupta, "Effect of  $\text{BCl}_3$  concentration and process pressure on the GaN mesa sidewalls in  $\text{BCl}_3/\text{Cl}_2$  based inductively coupled plasma etching," *Vacuum*, vol. 86, no. 12, pp. 1844–1849, Jul. 2012.
- [30] H. Hahn, J. B. Gruis, N. Ketteniss, F. Urbain, H. Kalisch, and A. Vescan, "Influence of mask material and process parameters on etch angle in a chlorine-based GaN dry etch," *J. Vac. Sci. Technol. A, Vac., Surf., Films*, vol. 30, no. 5, Sep. 2012, Art. no. 051302.



**Chengshiu Liou** received the B.S. and M.S. degrees from the Automatic Control Engineering Department, Feng Chia University, Taichung, Taiwan, Republic of China, in 2014 and 2016, respectively, where he is currently pursuing the Ph.D. degree with the Ph.D. Program of Electrical and Communications Engineering.

His current research interests include microelectromechanical systems and micro-LED display system.



**Fuchi Shih** was born in Taipei, Taiwan, Republic of China. He received the B.S. and M.S. degrees in engineering from the Automatic Control Engineering Department, Feng Chia University, Taichung, Taiwan, in 2018 and 2020, respectively. He is currently pursuing the Ph.D. degree with the Institute of NanoEngineering and MicroSystems, National Tsing Hua University (NTHU), Hsinchu, Taiwan.

His major research focuses on the MEMS and microprobe with thermal sensor integration.



**Yuanyuan Huang** received the M.S. degree from the Automatic Control Engineering Department, Feng Chia University, Taichung, Taiwan, Republic of China, in 2020. He is currently pursuing the Ph.D. degree with the Department of Power Mechanical Engineering, National Tsing Hua University (NTHU), Hsinchu, Taiwan.

His current research interests include MEMS and GaN on a silicon platform.



**Zihong Hu** received the B.S. and M.S. degrees from the Automatic Control Engineering Department, Feng Chia University, Taichung, Taiwan, Republic of China, in 2018 and 2020, respectively. He is currently pursuing the Ph.D. degree with the Institute of Nano Engineering and MicroSystems, National Tsing Hua University (NTHU), Hsinchu, Taiwan.

His current research interests include microelectromechanical systems and light-emitting diode packaging.



**Chingfu Tsou** received the M.S. and Ph.D. degrees in power mechanical engineering from National Tsing Hua University (NTHU), Hsinchu, Taiwan, Republic of China, in 1998 and 2003, respectively.

He is currently a Professor with the Department of Automatic Control Engineering, Feng Chia University, Taichung, Taiwan, and has more than two years of working experience in the field of MEMS and fingerprint sensor. His research interests include MEMS devices and systems, as well as MEMS/IC packaging technology.



**Weileun Fang** (Fellow, IEEE) was born in Taipei, Taiwan. He received the Ph.D. degree from Carnegie Mellon University, Pittsburgh, PA, USA, in 1995. His doctoral research focused on the determining of the mechanical properties of thin films using micromachined structures.

In 1995, he worked as a Post-Doctoral Research at the Synchrotron Radiation Research Center, Hsinchu, Taiwan. He joined the Power Mechanical Engineering Department, National Tsing Hua University, Hsinchu, in 1996, where he is currently a Chair Professor as well as a faculty of the NEMS Institute. In 1999, he was with Prof. Y.-C. Tai at California Inst. Tech. as a Visiting Associate. His research interests include MEMS with emphasis on microfabrication/packaging technologies, CMOS MEMS, CNT MEMS, micro-optical systems, microsensors and actuators, and characterization of thin-film mechanical properties.

Dr. Fang is currently the Chief Editor of JMM, the Associate Editor of the IEEE SENSORS JOURNAL, and the Board Member of the IEEE TRANSACTIONS ON DEVICE AND MATERIALS RELIABILITY. He served as a member of the International Steering Committee (ISC) of Transducers in 2009–2017, and the ISC Chair in 2017–2019. He also served as the General Chair of Transducers Conference in 2017. He was the TPC of the IEEE MEMS and EPC of Transducers for many years, and the Program Chair of the IEEE Sensors Conference in 2012. He served as the Chief Delegate of Taiwan for the World Micromachine Summit (MMS) in 2008–2012, and the General Chair of MMS in 2012. He has a close collaboration with MEMS industries and is now the VP of MEMS and Sensors Committee of SEMI Taiwan.